Nanotechnology **19** (2008) 455103 (8pp) doi:10.1088/0957-4484/19/45/455103

Rapid generation of protein aerosols and nanoparticles via surface acoustic wave atomization

Mar Alvarez, James Friend and Leslie Y Yeo

Micro/Nanophysics Research Laboratory, Department of Mechanical and Aerospace Engineering, Monash University, Melbourne, VIC 3800, Australia

E-mail: james.friend@eng.monash.edu.au

Received 29 June 2008, in final form 16 September 2008
Published 8 October 2008
Online at stacks.iop.org/Nano/19/455103

Abstract

We describe the fabrication of a surface acoustic wave (SAW) atomizer and show its ability to generate monodisperse aerosols and particles for drug delivery applications. In particular, we demonstrate the generation of insulin liquid aerosols for pulmonary delivery and solid protein nanoparticles for transdermal and gastrointestinal delivery routes using 20 MHz SAW devices. Insulin droplets around 3 μm were obtained, matching the optimum range for maximizing absorption in the alveolar region. A new approach is provided to explain these atomized droplet diameters by returning to fundamental physical analysis and considering viscous-capillary and inertial-capillary force balance rather than employing modifications to the Kelvin equation under the assumption of parametric forcing that has been extended to these frequencies in past investigations. In addition, we consider possible mechanisms by which the droplet ejections take place with the aid of high-speed flow visualization. Finally, we show that nanoscale protein particles (50–100 nm in diameter) were obtained through an evaporative process of the initial aerosol, the final size of which could be controlled merely by modifying the initial protein concentration. These results illustrate the feasibility of using SAW as a novel method for rapidly producing particles and droplets with a controlled and narrow size distribution.

1. Introduction

Biopharmaceutics are touted as a promising route to solve health issues in a myriad of ways from asthma, AIDS, influenza to cancer in rich and poor societies alike [1], yet the complexity of the biomolecules used and their study has limited progress, not only in the development of useful biopharma drugs, but also new production, manipulation, and delivery methods required to handle them. Furthermore, successful drugs are often so because of the ease in which they are delivered—painless, speedy, effective, and insignificant side effects represent attractive goals for any treatment. Non-invasive drug delivery is a popular means to achieve these goals, and doing so with biopharmaceuticals via inhaled, absorbed, or consumed aerosols and nanoparticles is an especially active research area. The dose efficiency and the number of possible delivery routes depend directly on the aerosol droplet and particle sizes. For generating such aerosols and particles with the requisite narrow size distributions for drug delivery applications, a MHz order surface acoustic wave (SAW) atomizer is proposed here. The production of liquid aerosols with sizes between 1 and 5 μm is ideally tailored for pulmonary delivery of therapeutic proteins and peptides [2], while the synthesis of 100 nm order protein nanoparticles is useful for transdermal and gastrointestinal delivery for inducing systemic responses and controlling biological processes [3].

Bovine serum albumin (BSA) solution and insulin were chosen as model drugs for aerosol generation in this study. The inhalation of regular insulin has been found to be a safe, painless and reliable alternative to subcutaneously injected insulin [4]. However, effectively delivering drugs into the body via the pulmonary system requires a controlled and narrow droplet size range: droplets smaller than 1 μm are mostly exhaled whereas the majority of droplets larger than 5 μm are deposited in the tracheobronchial region [5]. The 20 MHz SAW atomizers used in this work allow the generation of aerosol droplets within this narrow size range. Insulin and BSA may also be considered for non-invasive delivery via nanoparticles. The system described in this study produces nanoparticles through atomization and controlled evaporation

of the solvent in-flight [6, 7]; the nanoparticles have diameters generally below 100 nm and are therefore useful for these delivery methods.

SAW atomization offers advantages beyond controlled monodisperse aerosol and nanoparticle generation over other atomization techniques. The higher working frequency reduces the proclivity of the atomized drug to denature [8] and the established mass production techniques for high power SAW microdevices in the telecommunications industry [9] provides portable, scalable and low-cost devices.

2. Surface acoustic waves and interfacial destabilization

Rayleigh surface acoustic waves travel along the surface of an elastic material [10]; the elastic energy associated with their propagation is confined to within a few (4–5) wavelengths from the surface. As the Rayleigh wave passes through a point on the surface of a material, the point traces out an ellipse in a plane defined by the axis of the wave's propagation and an axis normal to the surface. The wave possesses two displacement components: a longitudinal component along the direction of propagation, and a transverse one perpendicular to the surface. These components can couple with a medium in contact with the SAW device. When the piezoelectric surface is in contact with a small volume of liquid, the longitudinal waves are diffracted into the liquid at an angle (i.e., the Rayleigh angle) $\theta_R = \sin^{-1}(c_l/c_s) \sim 22°$ due to the mismatch between the sound velocity in the solid c_s and in the liquid c_l, as illustrated in figure 1(a) [11–13]. At low amplitudes, the diffracted waves form longitudinal waves in the fluid along this direction. However, as the power is increased, a continuous flow may be induced in the fluid, known as acoustic *streaming* [13]; in a confined drop recirculation may be easily observed. As the acoustic wave power increases, however, other effects may be observed. The free surface may be caused to vibrate, the entire drop may be moved across the substrate, or simply atomized. Several applications involving relatively low power and low amplitude SAW have already been reported, including micromixing [14, 15], manipulation of small discrete droplets [12], and microparticle collection, concentration and dispersion [16, 17]. Increasing the power and vibration amplitude of the SAW, however, causes atomization of the drop to take place, resulting in a fine continuous mist of droplets ejected from the free surface of the drop [18].

The interaction of a vibrating solid with a liquid supported over the solid was first studied by Faraday in 1831. He vibrated liquid mercury in a tray at a few Hz, and found the wavelike disturbance created on the liquid surface was being induced at one-half the excitation frequency of the vibrating support [19]. A relationship for the capillary wavelength was subsequently derived by Kelvin [20]:

$$\lambda = \sqrt[3]{\frac{2\pi\gamma}{\rho f_c^2}}, \tag{1}$$

where γ and ρ are the surface tension and the density of the liquid, respectively, and f_c is the frequency of the surface waves.

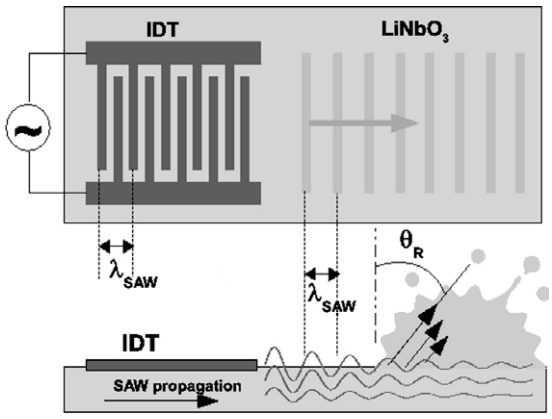

Figure 1. Schematic of the Rayleigh wave propagation and the atomization process.

After these initial observations, Lord Rayleigh experimentally confirmed Faraday's observations that the capillary waves on the liquid surface vibrated at one-half the frequency at which the support was excited, i.e. $f = 2f_c$ [21]. Later in 1962, Lang [22] proposed the following relationship based on a modification of (1) to predict the size of atomized droplets excited by ultrasonic vibration:

$$D = 0.34\sqrt[3]{\frac{8\pi\gamma}{\rho f^2}}, \tag{2}$$

where D is the droplet diameter and f is the applied frequency. The factor 0.34 is an empirically determined coefficient obtained for applied frequencies up to 1 MHz. Since then, this equation has been adopted for MHz order atomizers [23] and even high-frequency SAW atomizers, where good agreement was obtained only through modification of this empirical fitting coefficient [24].

Other models, both theoretical and empirical, have since been proposed to explain the mechanisms of droplet formation during atomization and predict the droplet size as a function of various combinations of the liquid density, viscosity, frequency, surface tension, and film thickness [25, 26]. For excitation frequencies on the order of 1 kHz, Vukasinovic *et al* [27] proposed that droplet ejection occurs as a result of the breakup of transient liquid spikes that are initiated by a collapse of free surface waves. Rayleigh instabilities are subsequently triggered along these spikes which then lead to pinch-off at the tip. Nevertheless, the mechanisms by which droplets are ejected under high-frequency ($\gg$1 kHz) excitation has only recently been proposed [28] to address discrepancies between experimental and theoretical results noted by some researchers [29].

In this paper, we first describe experiments to demonstrate the production of insulin liquid aerosols and solid protein nanoparticles using 20 MHz SAWs. Given the lack of physical models available that explain the characteristics of droplets formed via high-frequency atomization—beyond the near universal adoption of Lang's equation (2) that we have found to give diameters one order of magnitude smaller than observed in our experiments—we will also briefly discuss

possible scaling models to more accurately estimate droplet sizes.

3. Experimental details

3.1. SAW devices

The SAW devices used in this work have a single interdigital transducer (IDT) with 25 pairs of 400 nm thick, straight aluminium/titanium electrodes (fingers) sputter-deposited onto a single crystal 127.68° *yx*-cut lithium niobate ($LiNbO_3$, Roditi UK, London) piezoelectric substrate, as shown in figure 2(a). The IDT fabrication upon the piezoelectric substrate was performed using UV photolithography. The wavelength, λ, of the generated SAW is determined by the width of both the IDT electrode fingers and the gaps between them; in this simple configuration the gaps and finger widths were set to be equal and as a consequence the wavelength of the fundamental SAW is four times the finger width. For the chosen substrate, the wave propagation speed, c, is approximately 3965 m s^{-1}, and the frequency is given by $f = c/\lambda$. The SAW wavelength, λ_{SAW}, was chosen to be 200 μm, thus the device operating resonance frequency is set at 19.5 MHz (see figure 2(a)). In order to generate the SAW, a sinusoidal electrical signal matching the operating frequency is applied to the IDT using an RF signal generator (Agilent N9310A) and RF power amplifier (Faraday Pty. Ltd 10W1000C). The SAW generated with these devices have an amplitude of few nanometres as illustrated by the images (figure 2(b)) of the surface displacement normal to the substrate surface acquired using a laser Doppler vibrometer (LDV, Polytec MSA-400) while the SAW propagates from the IDT across the substrate.

3.2. Solution preparation

Two different proteins with very different molecular weights, insulin (MW = 5808 Da) and bovine serum albumin (BSA, MW = 66 430 kDa) were used. The insulin solution was prepared by dissolving 2 mg of bovine insulin powder (Sigma-Aldrich I5500) in 1 ml of DI water, with a pH of 2.15 (by adding 1 M HCl). The final pH was adjusted to 4 by adding 1 M NaOH. The BSA (Sigma-Aldrich A4919) was dissolved in DI water at the same concentration. A fixed volume of insulin or BSA solution was then delivered onto the SAW surface by using a syringe pump and subsequently atomized.

3.3. Droplet production and size characterization

A power sensor (Agilent U2004A) and condensation particle counter (CPC, TSI 3775) was used to determine the threshold power required to atomize a 2 μl liquid drop deposited upon the device surface. The atomization was carried out in a small chamber, and the droplets produced were collected using a 10 cm long flexible plastic tube connected to the CPC; the CPC drew the droplets along the tubing and into the machine for measurement. Three different liquid solutions were studied: DI water, 2 mg ml^{-1} BSA and 2 mg ml^{-1} insulin.

The size distribution of the ejected droplets was visually determined by collecting the insulin droplets on a Teflon-coated (Teflon AF, Dupont Corp.) glass slide. The Teflon coating prevented localized spreading of these droplets and associated droplet coalescence on the slide during collection. A high-speed video camera (iSpeed, Olympus) connected to a boom microscope (BXFM, Olympus) was used to image the droplets falling onto the Teflon-coated slide. The videography allowed the exclusion of external effects, such as the coalescence of the collected droplets or droplet evaporation when determining the size of the collected droplets using image processing software (ImageJ, National Institutes of Health, USA).

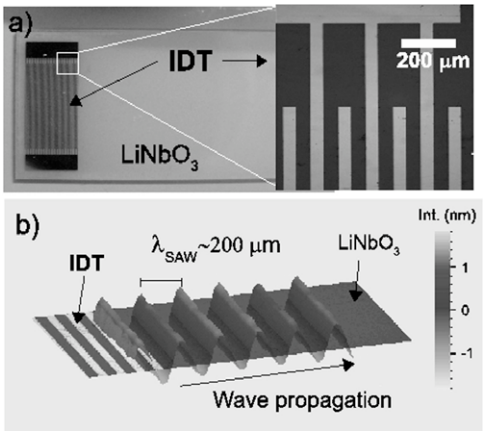

Figure 2. (a) Image of the fabricated SAW device. The inset shows a magnification of the fabricated interdigital transducers patterned on the substrate, with edge of the bus bar at top, finger tip–bus bar gap in the middle, and electrode fingers at bottom. (b) SAW propagating along the x axis of the SAW substrate as imaged using laser Doppler vibrometry; the measured displacement is only the component transverse to the surface (the longitudinally polarized component cannot be measured with our LDV). Note the vertical scale is greatly exaggerated for clarity.

3.4. Nanoparticle production and size characterization

Nanoparticles were prepared by allowing the atomized droplets to evaporate in-flight. The setup consists of a glass tube heated with hot water (70 °C), connected on one side to a glass chamber, where the SAW is located, and on the other to a vacuum pump (1.5 l min^{-1}) to extract the particles (figure 3). The particles were sized by collecting them on an atomically flat mica substrate (Grade V–4, SPI Supplies) located at the end of the heated glass tube. With this setup, the particles travel a distance of 34 mm along the heated tube before impacting the substrate; the configuration is simple, hinting at the practicality of this approach. This length is sufficient for the solvent to evaporate and the particles to harden before impacting the substrate without splattering. A scanning electron microscope (SEM, Hitachi S570) was used to measure the size of the collected particles. Again, *Image J* was used to analyse the SEM images and to determine the particle size distribution.

4. Results and discussion

4.1. Aerosol generation

The atomization process as photographed at 2000 fps is shown in figure 4. Due to the hydrophilicity of the substrate, the

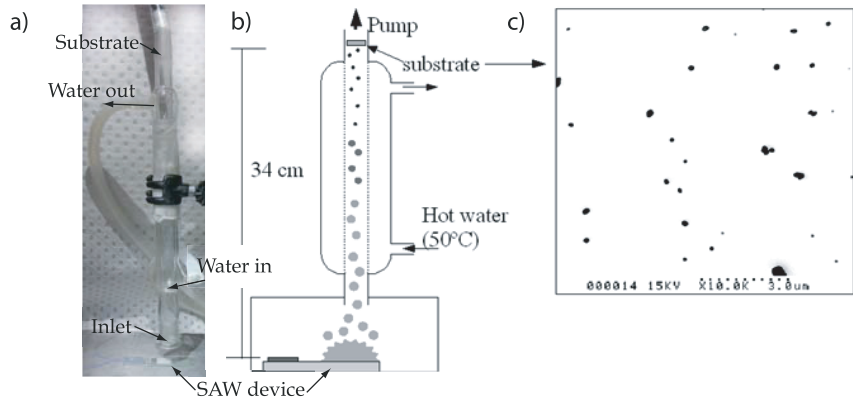

Figure 3. (a) Photograph and (b) schematic of the drying configuration, and, (c) typical SEM image of the particles collected on the substrate.

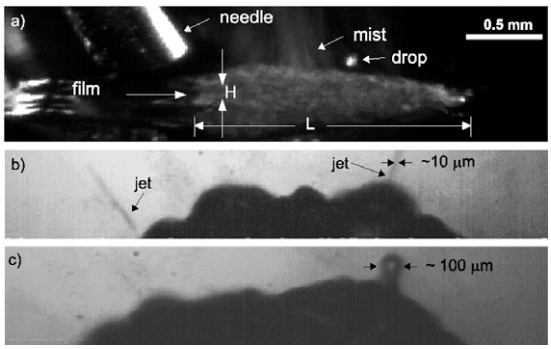

Figure 4. (a) Representative image of the capillary waves created over a water drop surface, obtained using a high-speed video camera. The images below are a magnification of the surface instabilities (lateral view) which show, (b) the ejection of jets responsible for the smaller 1–10 μm droplets ejected, and, (c) the crest elongation responsible for the pinch-off of the larger 100 μm ejected droplets.

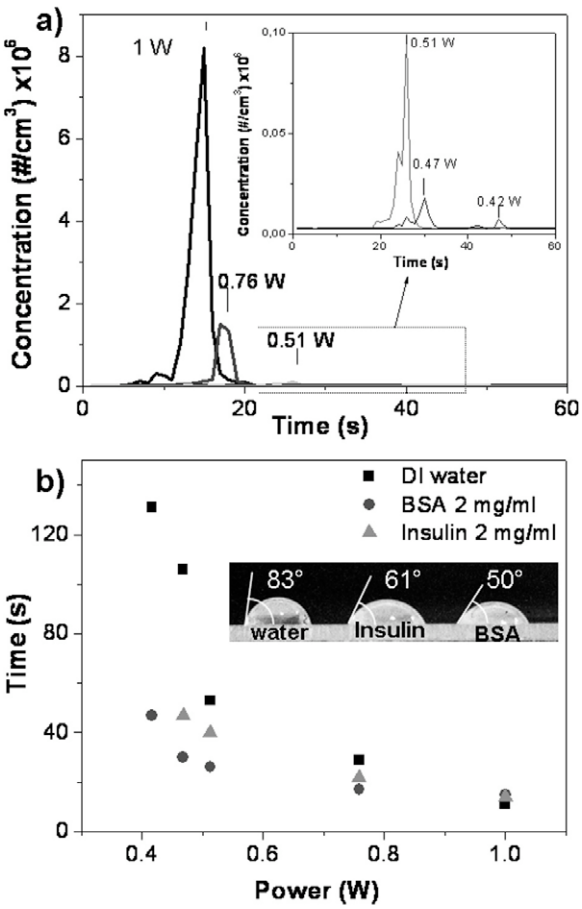

Figure 5. (a) Number of droplets per cm^2 produced during the atomization of 2 μl of BSA as function of the applied power, and, (b) time corresponding to the maximum peak of the detected droplets as function of the applied power. The inset shows the contact angles for DI water, insulin and BSA drops.

deposited drop first spreads into a thin elongated film with height $H \sim 0.2$ mm and length $L \sim 2$ mm ($\gg\lambda_{SAW}$) on the surface when the SAW appears on the substrate (figure 4(a)). Individual jets form soon after due to a gross destabilization of the fluid free surface, each of which eventually breaks up to form small droplets (figure 4(b)). At the same time, a continuous mist of 1–10 μm droplets is produced in the background above the free surface of the parent drop, similar to those observed by Barreras *et al* [29]. This mist is probably due to 1–10 μm diameter jets that emanate from the drop free surface at many different locations. From time to time, the ejection of larger droplets (~100 μm) was also observed due to large 100 μm order capillary waves induced at the free surface that subsequently pinch-off as shown in figure 4(c). Because of their size, these ejected drops quickly return either back onto the parent drop or to another point on the substrate.

4.2. Aerosol characterization

The mist consisting of the 1–10 μm droplets produced was studied as a function of the applied power for three different solutions: DI water, BSA and insulin. The results obtained with the CPC and the power sensor show that, in all cases, the number of droplets ejected decrease with a reduction in the power of the input signal. Figure 5(a) shows the number of BSA droplets generated per cm^3, representative of the other cases (not shown). This is because the drop that is initially deposited onto the surface must spread into a thin film similar

to that shown in figure 4(a) before atomization may occur. As such, we observe a time delay of between 5 and 50 s before the peaks that indicate the presence of the atomized droplets are observed in figure 5(a). This time lag is due in part to the drop spreading but also due to the time it takes for the ejected droplets to travel to the detector in the CPC. We note that the time lag increases as the applied power decreases since the drop spreads more slowly under the action of the SAW induced beneath it.

If we plot the time at which the maximum concentration of the detected drops appears as a function of the applied power for the three fluids, i.e., around 20 s in figure 5(a), there is a clear dependence of this time on the applied power as shown in figure 5(b). The time decreases with decreasing surface tension of the solution, supporting the idea that the drop must spread into a film before atomization may occur. The surface tension is reduced as the concentration of the protein dissolved increases [30]; this is why the BSA and insulin solution droplets have lower measured contact angles than water as shown in the inset of figure 5(b). As the surface tension decreases, the drop not only spreads more quickly (therefore reducing the time lag) but also more easily into a thinner film. Since it is easier to destabilize the interface of a thin liquid film as opposed to a thicker one, we observe the number of detected droplets to increase with decreasing surface tension. It should be noted that the surface tension of insulin is dependent on the pH in addition to the insulin concentration, due to the tendency of bovine insulin to aggregate [31], and so the contact angle of the insulin drop can vary considerably.

Since the time delay prior to the commencement of atomization increases at lower applied powers, allowing time for the parent drop to evaporate before it atomizes, we use a power of around 30 dBm (1 W) in the following experiments to minimize evaporation effects. Figure 6 shows a typical droplet size distribution obtained for DI water, with a droplet mean diameter of about 3.2 μm. We observe the distribution to be quite monodisperse which is essential to minimize drug loss in the generation of aerosols for inhalation therapy. Slightly lower diameters would be expected for the insulin and BSA solutions (due to the lower surface tension); however, similar values are obtained due to the resolution limitation of our imaging technique. In any case, the obtained values match the 1–5 μm range required for optimal deposition of aerosols in the lower respiratory tract.

4.3. Replacing Lang's equation

The 1–10 μm droplet diameters obtained are an order of magnitude larger than that predicted by Lang's equation in (2). Lang arrived at his equation presuming the capillary waves will vibrate at half the excitation frequency, i.e. $f_c = f/2$, consistent with Faraday and Rayleigh's experiments on the formation of capillary waves at the liquid surface due to vibration normal to the liquid surface, and rather sophisticated analyses that have appeared subsequently [32]—indeed such subharmonic waves are termed *Faraday waves*. For SAW-driven atomization, however, there is no particular reason to believe this subharmonic relation is relevant [28]. The SAW

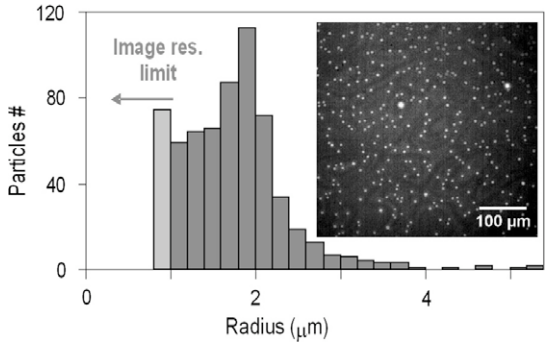

Figure 6. Typical size distribution of atomized insulin droplets collected on a Teflon-coated glass slide; the 'particles #' refers to the number of droplets in the image falling into each diameter range; the bins in the histogram are 0.2 μm wide.

propagates along the substrate, and upon encountering the droplet, diffracts into the liquid drop at the Rayleigh angle, rather different than the piston-like inducement of the Faraday wave. Further, we employ far higher excitation frequencies than the few Hz to kHz order frequencies used in past studies. As such, there is little reason for us to believe why (2) is relevant in our case, as has been assumed in previous SAW atomization studies [24].

This judgement is supported by the images of the capillary waves induced on the free surface of the thin film prior to atomization, as shown in figure 7. Also shown are measurements of the capillary wave profile using a grey scale pixel intensity analysis with ImageJ. We observe that two dominant capillary wavelengths are excited at the free surface, one at 200 μm and the other around 10 μm, for both the BSA solution and water. We note that the 200 μm capillary wavelength corresponds to the wavelength of the 20 MHz SAW on the substrate. Had the $f_c = f/2$ subharmonic been parametrically excited at the free surface, we would have obtained a capillary wavelength double this value. In any case the 200 μm capillary waves suggest why the large 100 μm order droplets are ejected as shown in figure 7(c).

The shorter 10 μm capillary wavelength suggests why the 1–10 μm order droplets diameters arise in the form of the continuous mist seen in figure 4(b). Specifically, these 10 μm order capillary waves are destabilized into inertially-driven jets of the same diameter that eventually break up into droplets due to axisymmetric instabilities that are triggered along the length of the inertially-driven elongation of the jet.

In place of (2), we propose a simple scaling analysis arising from a viscous-capillary dominant force balance to predict the instability wavelength [28]:

$$\lambda \sim \frac{\gamma H^2}{\mu f_c L^2}, \tag{3}$$

where μ is the fluid viscosity, and H and L are the vertical and lateral dimensions of the drop, respectively. When atomizing a drop, $H/L \sim 1$. However, in our experiments, due to the spreading of the drop into a film, $H/L \sim 10^{-1}$. An instability wavelength value between 1 and 10 μm is then obtained for $\mu \sim 10^{-3}$ kg ms^{-1}, $\gamma \sim 10^{-2}$ N m^{-1} and $f_c \sim 10$ kHz, on the

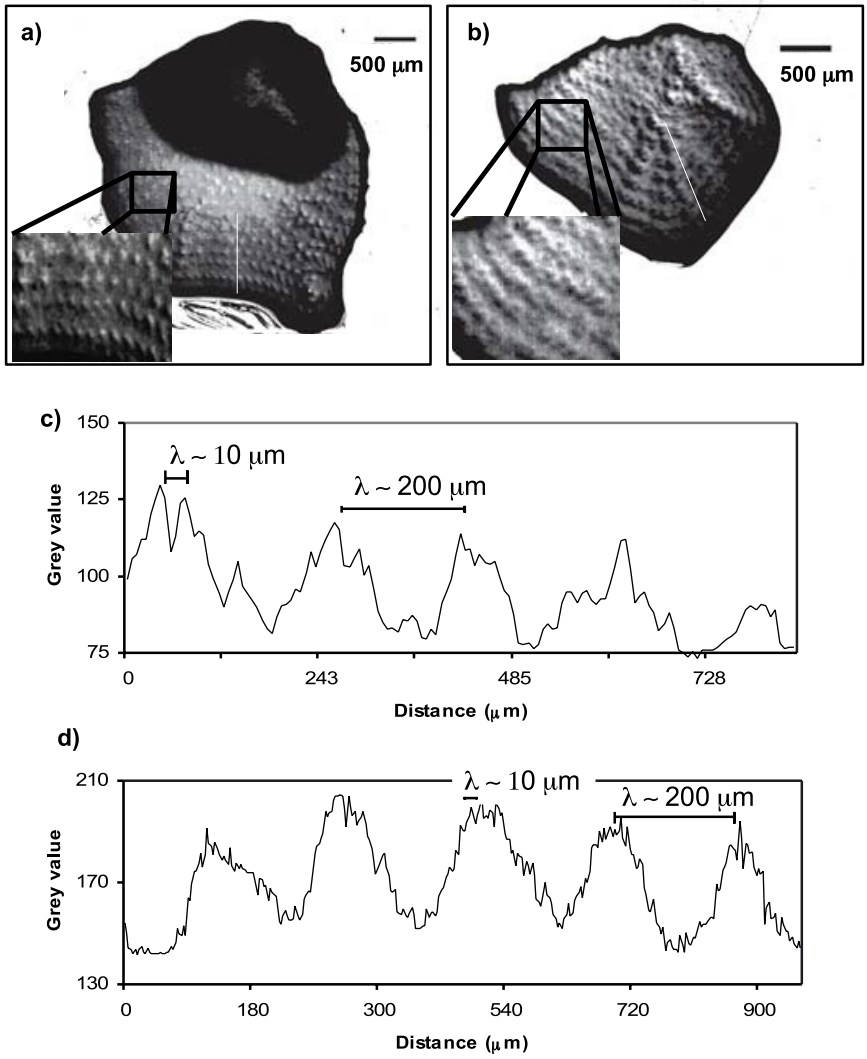

Figure 7. Plan view images of the parent drop of (a) BSA, and, (b) water, which have spread into a thin film on the substrate just prior to atomization. Below are the capillary wave profiles from images (a) and (b) measured using ImageJ, indicating that the primary wavelength of the capillary wave is around 200 μm and the secondary wavelength is around 10 μm.

order of the observed capillary wavelength in figure 7 and the dimensions of the smaller droplets.

4.4. Nanoparticle production and characterization

Both the BSA and insulin solutions were able to be atomized and evaporated to form nanoparticles. The histograms obtained for the particle size distribution shown in figure 8 suggest mean particle radii of 110 nm and 65 nm for insulin at concentrations of 2 mg ml^{-1} and 0.5 mg ml^{-1}, respectively, while radii of 80 and 60 nm were obtained for BSA for the same respective concentrations.

The expected particle size, R_p, can be estimated from the initial droplet size, R_d, by assuming that all the protein in one droplet crystallizes into a single spherical particle [33]:

$$R_p = R_d \sqrt[3]{C/\rho_p}, \tag{4}$$

where C is the initial protein concentration and ρ_p is the protein density. For the aerosols generated previously, a mean radius of about 1.5 μm was obtained. Estimating the density of the protein to be 1500 mg ml^{-1} [34], the particle radius is about 165 nm when using a solution of insulin of 2 mg ml^{-1}, which agrees reasonably well with the experimental value of 110 nm, considering the error in the droplet measurement and the possible loss of some of the protein during atomization (e.g., through adsorption onto the substrate). These results show the possibility of controlling the final size of the particles solely through the modification of the source drop's protein concentration.

Assuming that the density of the crystallized protein does not change with the initial concentration, we expect the radius of the particle to decrease with the cube root of the mass ratio. That means that for the two different concentrations used in this work, i.e., 2 and 0.5 mg ml^{-1}, a particle size ratio of 1.58 is expected for each protein: $(2)R_p/(0.5)R_p = \sqrt[3]{(2)C/(0.5)C}$. The experimental size ratio obtained for insulin and BSA were 1.69 and 1.33, respectively, close to the theoretical prediction. The different particle sizes for different proteins and the

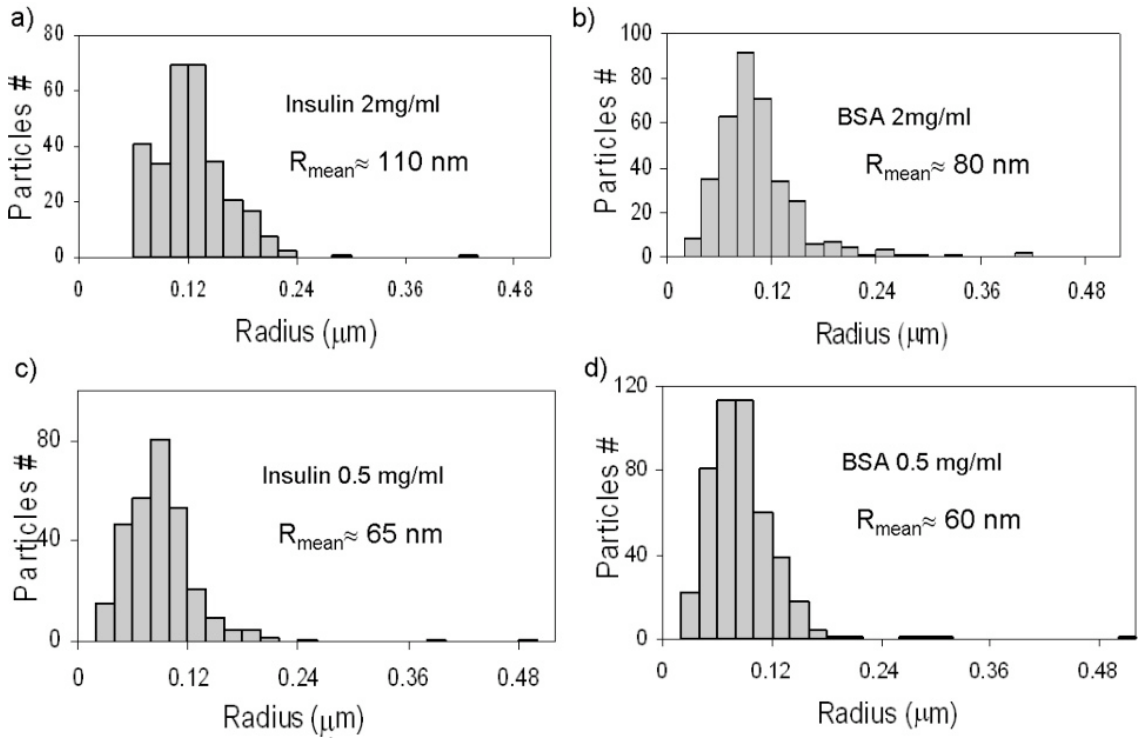

Figure 8. (a) Size distribution of the collected insulin and BSA particles for an initial concentration in solution of 2 mg ml^{-1} and 0.5 mg ml^{-1}.

deviation from the theoretical prediction are attributed to the possible dependency of the protein density on its molecular weight [34] and the effect of the protein solubility (surface tension and viscosity) and net molecular charge (positive for BSA and negative for insulin) on the size of the initial ejected droplet.

5. Conclusions

In summary, a straightforward and rapid method to generate monodisperse and uniform liquid aerosols and nanoparticles for drug delivery applications has been described. This method is able to generate protein-loaded liquid aerosols in the optimal range for effective pulmonary absorption. In addition, 50–100 nm diameter protein particles for transdermal or buccal delivery can also be produced [3, 35]. Relative to other generation methods, this is a flexible and reliable method allowing the rapid generation of aerosols and powders of drugs without mechanically moving parts. As such, we propose the SAW technology as a rapid and simple alternative for the development of a low power portable device both for the pulmonary delivery of liquid insulin or other therapeutic agents—peptides, proteins, siRNA, DNA, and vaccines—and for the generation of drug nanoparticles for other non-invasive delivery routes.

Acknowledgments

This work was supported by grant BN004 from Nanotechnology Victoria, and Australian Research Council Discovery Project grants DP0666660 and DP0773221.

References

[1] Buxton M, Hanney S and Jones T 2004 Estimating the economic value to societies of the impact of health research: a critical review *Bull. World Health Organ.* **82** 733
[2] Agu R U, Ugwoke M I, Armand M, Kinget R and Verbeke N 2001 The lung as a route for systemic delivery of therapeutic proteins and peptides *Respir. Res.* **2** 198–209
[3] McAllister D V, Wang P M, Davis S P, Park J-H, Canatella P J, Allen M G and Prausnitz M R 2003 Microfabricated needles for transdermal delivery of macromolecules and nanoparticles: fabrication methods and transport studies *Proc. Natl Acad. Sci. USA* **100** 13755–60
[4] Patton J S, Bukar J and Nagarajan S 1999 Inhaled insulin *Adv. Drug Deliv. Rev.* **35** 235–47
[5] Groneberg D A, Witt C, Wagner U, Chung K F and Fischer A 2003 Fundamentals of pulmonary drug delivery *Respir. Med.* **97** 382–7
[6] Yeo L Y, Gagnon Z and Chang H-C 2005 Ac electrospray biomaterials synthesis *Biomaterials* **26** 6122–8
[7] Friend J R, Yeo L Y, Arifin D R and Mechler A 2008 Evaporative self-assembly assisted synthesis of polymeric nanoparticles by surface acoustic wave atomization *Nanotechnology* **19** 145301
[8] Li H, Friend J R and Yeo L Y 2007 A scaffold cell seeding method driven by surface acoustic waves *Biomaterials* **28** 4098
[9] Hashimoto K Y 2000 *Surface Acoustic Wave Devices in Telecommunications: Modelling and Simulation* (Berlin: Springer)
[10] White R and Voltmer F 1965 Direct piezoelectric coupling to surface elastic waves *Appl. Phys. Lett.* **7** 314–6
[11] Shiokawa S, Matsui Y and Ueda T 1990 Study on saw streaming and its application to fluid devices *Japan. J. Appl. Phys.* **28** (suppl. 29–1) 137–9
[12] Wixforth A, Strobl C, Gauer Ch, Toegl A, Scriba J and Guttenberg Z V 2004 Acoustic manipulation of small droplets *Anal. Bioanal. Chem.* **379** 982–91

[13] Chono K, Shimizu N, Matsui Y, Kondoh J and Shiokawa S 2004 Development of novel atomization system based on saw streaming *Japan. J. Appl. Phys.* **43** 2987–91
[14] Sritharan K, Strobl C J, Schneider M F and Wixforth A 2006 Acoustic mixing at low Reynold's [sic] numbers *Appl. Phys. Lett.* **88** 054102
[15] Shilton R, Tan M K, Yeo L Y and Friend J R 2008 Particle concentration and mixing in microdrops driven by focused surface acoustic waves *J. Appl. Phys.* at press
[16] Tan M K, Friend J R and Yeo L Y 2007 Microparticle collection and concentration via a miniature surface acoustic wave device *Lab Chip* **7** 618–25
[17] Li H, Friend J R and Yeo L Y 2007 Surface acoustic wave concentration of particle and bioparticle suspensions *Biomed. Microdev.* **9** 647–56
[18] Kurosawa M, Watanabe T and Higuchi T 1995 Surface acoustic wave atomizer with pumping effect *IEEE Micro Electro Mechanical Systems (Amsterdam)* pp 25–30
[19] Faraday M 1831 On the forms and states assumed by fluids in contact with vibrating elastic surfaces *Phil. Trans. R. Soc. Lond.* **52** 319–40
[20] Kelvin L 1871 Hydrokinetic solutions and observations *Phil. Mag.* **42** 362–77
[21] Rayleigh L 1883 On the crispations of fluid resting upon a vibrating support *Phil. Mag.* **15** 50–8
[22] Lang R J 1962 Ultrasonic atomization of liquids *J. Acoust. Soc. Am.* **34** 6–8
[23] Forde G, Friend J R and Williamson T 2006 Straightforward biodegradable nanoparticle generation through megahertz-order ultrasonic atomization *Appl. Phys. Lett.* **89** 064105
[24] Kurosawa M, Futami A and Higuchi T 1997 Characteristics of liquids atomization using surface acoustic wave *IEEE Transducers'97* pp 801–4
[25] Rajan R and Pandit A B 2001 Correlations to predict droplet size in ultrasonic atomization *Ultrasonics* **39** 235–55
[26] James A J, Vukasinovic B, Smith M K and Glezer A 2003 Vibration-induced drop atomization and bursting *J. Fluid Mech.* **476** 1–28
[27] Vukasinovic B, Smith M K and Glezer A 2007 Mechanisms of free-surface breakup in vibration-induced liquid atomization *Phys. Fluids* **19** 012104
[28] Qi A, Friend J R and Yeo L Y 2008 Interfacial destabilization and atomization driven by surface acoustic waves *Phys. Fluids* at press
[29] Barreras F, Amaveda H and Lozano A 2002 Transient high-frequency ultrasonic water atomization *Exp. Fluids* **33** 405–13
[30] Okubo T and Kobayashi K 1998 Surface tension of biological polyelectrolyte solutions *J. Colloid Interface Sci.* **205** 433–42
[31] Lin F Y H, Kwok D Y, Policova Z, Zingg W and Neumann A W 1995 The effect of ph and concentration on the surface tension of adsorbed layers of various insulin preparations *Colloids Surf.* B **3** 281–6
[32] Miles J W 1984 Nonlinear Faraday resonance *J. Fluid Mech.* **146** 285–302
[33] Leong K H 1987 Morphological control of particles generated from the evaporation of solution droplets: theoretical considerations *J. Aerosol Sci.* **18** 511–24
[34] Fischer H, Polikarpov I and Craievich A F 2004 Average protein density is a molecular-weight-dependent function *Protein Sci.* **13** 2825–8
[35] Luo Y, Xu H, Huang K, Gao Z, Peng H and Sheng X 2005 Study on a nanoparticle system for buccal delivery of insulin *IEEE Engineering in Medicine and Biology 27th Annual Conf. (Shanghai)* pp 4842–5